Characteristics of aerosol optical properties in pollution and Asian dust episodes over Beijing, China

Chenbo Xie,[1,2] Tomoki Nishizawa,[2,*] Nobuo Sugimoto,[2] Ichiro Matsui,[2] and Zifa Wang[3]

[1]Atmospheric Environment Division, National Institute for Environmental Studies, Tsukuba, Ibaraki, 305-8506, Japan

[2]Center for Atmospheric Optics, Anhui Institute of Optics and Fine Mechanics, Chinese Academy of Sciences, Hefei, Anhui, 230031, China

[3]Institute of Atmospheric Physics, Chinese Academy of Sciences, Beijing, 100029, China

*Corresponding author: nisizawa@nies.go.jp

Received 4 April 2008; revised 4 August 2008; accepted 12 August 2008; posted 12 August 2008 (Doc. ID 94691); published 17 September 2008

Aerosol optical properties were continuously measured with the National Institute for Environmental Studies (NIES) compact Raman lidar over Beijing, China, from 15 to 31 December 2007. The results indicated that in a moderate pollution episode, the averaged aerosol extinction below 1 km height was $0.39 \pm 0.15\,km^{-1}$ and the lidar ratio was 60.8 ± 13.5 sr; in heavy pollution episode, they were $1.97 \pm 0.91\,km^{-1}$ and 43.7 ± 8.3 sr; in an Asian dust episode, they were $0.33 \pm 0.11\,km^{-1}$ and 38.3 ± 9.8 sr. The total depolarization ratio was mostly below 10% in the pollution episode, whereas it was larger than 20% in the Asian dust episode. The distinct characteristics of aerosol optical properties in moderate and heavy pollution episodes were attributed to the difference in air mass trajectory and the ambient atmospheric conditions such as relative humidity.

OCIS codes: 010.0010, 010.3640, 120.0280, 280.0280, 280.1120, 280.3640.

1. Introduction

Air pollution has long been a problem in the industrial nations of the West. It has now become an increasing source of environmental degradation in the developing nations of East Asia. Because of its rapid push to industrialize, China in particular is experiencing dramatic levels of air pollution over a large portion of the country [1]. As the capital of China and one of its biggest cities, Beijing is representative of urban air pollution in China. Soot, vehicle exhaust gas emissions, and other pollutants frequently cover up the former azure blue of Beijing's sky. Meanwhile, Beijing has also been experiencing increasingly severe Asian dust storms in the spring, due to its special geographical location. Asian dust storms are composed of mineral particles lifted from the arid regions in north China and Mongolia, and they are easily transported to Beijing by the westerlies during the spring season. Previous research demonstrated that Asian dust particles play significant roles in the climate, as do anthropogenic aerosols [2]. Thus, quantitative measurements of polluted aerosols and Asian dust particles over Beijing are very important and necessary in air pollution abatement and Asian dust studies.

Raman lidar permits the independent measurement of aerosol extinction and backscatter by detecting the elastic and Raman scattering signals [3], and it has been widely and successfully used for quantitative observations of aerosols [4–9], especially in continuous and automatic operation [10]. But Raman lidar measurements in Beijing are very rare. The field campaign in January of 2005 reported by Tesche *et al.* [11] is only one observation; however, they captured neither typical air pollution nor Asian dust cases during their short 11 day experiment. To obtain

0003-6935/08/274945-07$15.00/0

the optical parameters for typical aerosol events in Beijing is one of our motivations for the long-term Raman lidar observation presented in this paper.

The National Institute for Environmental Studies (NIES) compact Raman lidar system operating in Beijing is part of the lidar network established by NIES for monitoring polluted aerosols and Asian dust [12,13]. The lidar site is located at the Institute of Atmospheric Physics, Chinese Academy of Sciences in Beijing, China (39.97 N, 116.37 E). For this study, Raman lidar measurements included moderate and heavy pollution, as well as the Asian dust episodes that occurred from 15 to 31 December 2007. The results of our analysis are presented here. Section 2 describes the NIES compact Raman lidar system and the data analysis procedure. Section 3 presents typical profiles of optical properties for polluted aerosols and Asian dust particles, and Section 4 gives a summary and discussion.

2. NIES Compact Raman Lidar and Data Analysis Method

NIES compact Raman lidar operates in a continuous mode (5 min of data acquisition with 10 min intermissions) through a window on the roof of the observation room, regardless of weather. The lidar system employs a Nd:YAG laser (Quantel, Brilliant Ultra) as a light source that generates the fundamental output at 1064 nm and the second harmonic at 532 nm. Transmitted laser energy is typically 40–50 mJ per pulse at 1064 nm and 10–20 mJ per pulse at 532 nm. The pulse repetition rate is 10 Hz. A 20 cm diameter Schmidt–Cassegrain telescope (Celestron, C8-A XLT) with a field of view of 1 mrad is used to collect the backscattered light. The receiver has four detection channels to receive the return signal at 1064 nm, nitrogen Raman scattering at 607 nm, and parallel and perpendicular polarization components at 532 nm. The optical bandwidth of each channel is 1 nm at 1064 nm, 3 nm at 607 nm, and 1 nm for two polarization channels at 532 nm.

An analog-mode avalanche photodiode (Licel, APD-1.5) is used as a detector for 1064 nm, and two photomultiplier tubes (PMTs) (Hamamatsu, H6780-02) are used for the parallel and perpendicular polarization components at 532 nm. The detected signals are recorded with 12 bit transient digitizers (Turtle Industry, TUSB-0212ADM) with a sampling rate of 25 MHz, corresponding to a range resolution of 6 m. The data are transferred to a PC and averaged for 3000 laser shots (5 min) during continuous observation. A PMT module for photon counting with a thermoelectric cooler (Hamamatsu, H7421-40) is used as a detector for the Raman scattering channel at 607 nm. The photoelectron signals produced by the PMT are counted by a multichannel scaler board (SigmaSpace AMCS-usb) with 50 ns time gates, corresponding to a range resolution of 7.5 m. The signals are accumulated for 3000 laser shots on the board and transferred to the PC. Though the signals from the Raman channel were recorded both in day and night, only nighttime data (from 18:00 to 4:00 local time) were used in the analysis because of the large background radiation in the daytime. The range resolution was reduced to 30 m in the data processing for both of the elastic and the Raman signals.

The total depolarization ratio is defined as the ratio of the perpendicular polarization component to the parallel component of the backscattered signals, and it is a useful indicator of nonsphericity for identifying ice clouds [14] and dust layers [15]. In order to calibrate the sensitivity of the two polarization channels, a linear polarizer sheet directed at an angle of 45 ° was inserted in front of the polarization cube before the experiment, and the gains of the two PMTs were balanced.

The aerosol extinction coefficient at the laser wavelength of 532 nm was calculated from the Raman scattered signal and the number density of the atmospheric molecules with an assumption of the wavelength dependence of aerosol extinction $\alpha_a \propto \lambda^{-k}$, here $k = 0$ for dust aerosol [3] and 1 for pollution aerosol [16]. The molecular number density was derived from the daily radiosonde data launched at 1100 UTC from the Meteorological Station in Beijing [International Civil Aviation Organization (ICAO) location indicator: Beijing Capital Airport (ZBAA), 39.93 N, 116.28 E]. A sliding linear least-square fit with a 150 m window was applied in the derivation of the logarithm of the ratio of the atmospheric number density to the range-corrected Raman signal. To reduce the error in the derived aerosol extinction coefficient, the range-corrected Raman lidar signals were averaged for 2 h and also spatially smoothed with a height-dependent range resolution, which linearly increases from 120 m at 500 m height to 600 m at 2 km.

The backscatter ratio, defined as the ratio of the total (aerosol plus molecular) to molecular backscatter coefficients, was calculated from the elastic and Raman signals. It was normalized at the aerosol-free ranges where the aerosol backscattering was expected to be negligible. In the heavy pollution and dust cases, however, the intensity of Raman signals was not sufficiently high at the ranges. Under such conditions, we used the lidar system constant determined in the clear conditions to calibrate the sensitivity of the elastic and Raman detection channels. We used the data in the clear free troposphere (4 to 5 km) on 31 December to determine the system constant in this study. We assumed the backscatter ratio was 1.1 at the calibration altitudes. The aerosol backscatter coefficient was then derived from the backscatter ratio and the molecular backscatter coefficient calculated from the radiosonde temperature and pressure data.

The aerosol lidar ratio (aerosol extinction-to-backscatter ratio) was calculated by taking the ratio of the aerosol extinction coefficient to the backscatter coefficient. As is well known, the lidar ratio is an important parameter for retrieving extinction coefficient from the elastic-backscatter lidar signals, and it is

also a useful parameter for characterizing microphysical properties of aerosols such as size distribution, refractive index, and particle shape [17–19].

At the lower height, the geometrical form factor correction was applied. The overlap function was determined from the measured Raman signal and the molecular density profile after applying molecular and aerosol extinction correction to the Raman profile [20]. To minimize the error caused by the assumption of the constant lidar ratio in the lower heights, the data in the clear conditions on 31 December were used in this study for determining the overlap function. The large error in the overlap correction was expected in the heights below 200 m, we did not use the derived optical parameters below 200 m height.

3. Results

Figure 1(a) depicts the comparison of the daily lidar aerosol extinction coefficient and the surface mass concentration of particulate matter smaller than 10 μm (PM_{10}) during the experiment. The aerosol extinction coefficient was derived from the lidar measurement from 1000 to 2000 UTC with a 2 h temporal resolution and averaged in the range of 0.2 to 0.3 km. The mass concentration of PM_{10} was converted from the reported air pollution index in Beijing city that was averaged from 1200 LT of the previous day to 1200 LT of that day. The date indicated in Fig. 1 is the date for the lidar measurement,

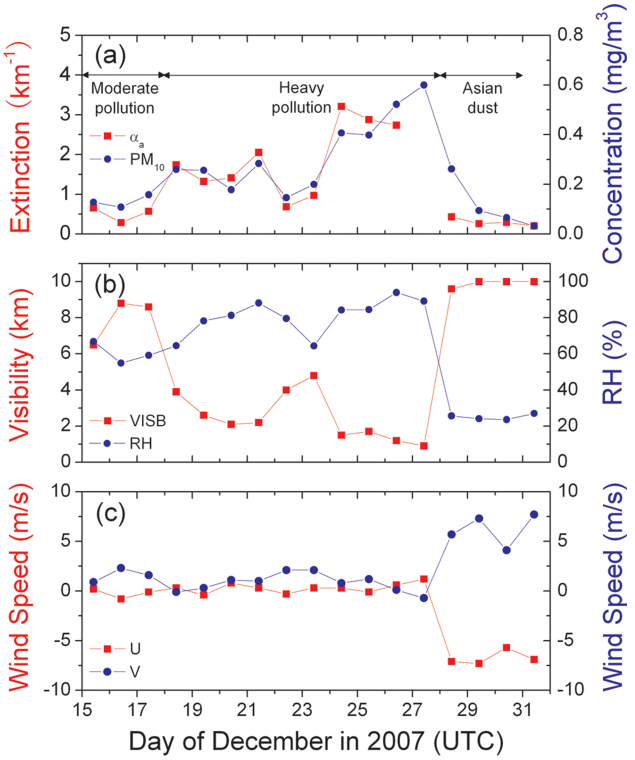

Fig. 1. (Color online) Daily variation of the lidar aerosol extinction coefficient α_a (0.2–0.3 km), surface mass concentration of PM_{10}, visibility, relative humidity, and wind speed and direction during the experiment from 15 to 31 December 2007 in Beijing.

and the date for the PM_{10} measurement is shifted one day ahead so that the timing of the lidar measurement is in the averaging period for PM_{10}. On 27 December, the lidar extinction coefficient is missing because the extinction was too large and it was difficult to analyze the Raman scattering signals.

As can be seen in Fig. 1(a), the measured aerosol extinction coefficient and PM_{10} are correlated very well except for 28 December. The observed lidar depolarization ratio showed an Asian dust event occurred on that day. The difference between the extinction coefficient and PM_{10} is mainly due to the difference in the period of the measurement. Another possible reason is the mass/extinction ratio is larger for large Asian dust particles.

Surface visibility, relative humidity, and wind speed and direction at the ZBAA Meteorological Station are also shown in Figs. 1(b) and 1(c). In these plots, the visibility and relative humidity were averaged between 1000 and 2000 UTC (the same period with the lidar measurement), and the wind speed was averaged for one day in the same way as for the PM_{10} data. The meteorological data indicate that the condition with a high relative humidity (>50%), and low wind speed (<2.5 m/s) stayed from 15 to 27 December. On 28 December, a strong northwesterly at 10 m/s prevailed and continued to 31 December. The surface visibility had a reasonable negative correlation with the aerosol extinction coefficient. Note that the instrument upper limit of the visibility was 10 km. According to the aerosol extinction coefficient and the meteorological data, we may classify the situations that occurred in the experiment period into three episodes, namely a moderate pollution episode from 15 to 17 December, a heavy pollution episode from 18 to 27 December, and an Asian dust episode from 28 to 30 December. The characteristics of aerosol optical properties in these three episodes are analyzed and discussed in the following subsections.

A. Moderate Pollution Episode

Figure 2(a) shows aerosol extinction and backscatter coefficients, the lidar ratio, and the total depolarization ratio observed on 16 December during a moderate pollution episode. The aerosol extinction decreased gradually from 0.3 km^{-1} near the surface to 0.1 km^{-1} at a height of 0.9 km. Over 0.9 km height, it was difficult to derive aerosol extinction from the Raman signals due to the low signal-to-noise ratio. The aerosol backscatter profile reached about 3 km, and the values fluctuated around zero above this height. The averaged lidar ratio below 0.9 km was 73.9 $\pm$ 6.1 sr, and the corresponding total depolarization ratio was 5.67 $\pm$ 0.50%.

A high lidar ratio and a low total depolarization ratio suggest the presence of light-absorbing spherical aerosol species such as soot [21]. Soot is released from incomplete combustion of carbonaceous fuels, and it is frequently found in Beijing during the heating period in winter [22]. To estimate the possible sources of aerosols, the four-day backward trajectory

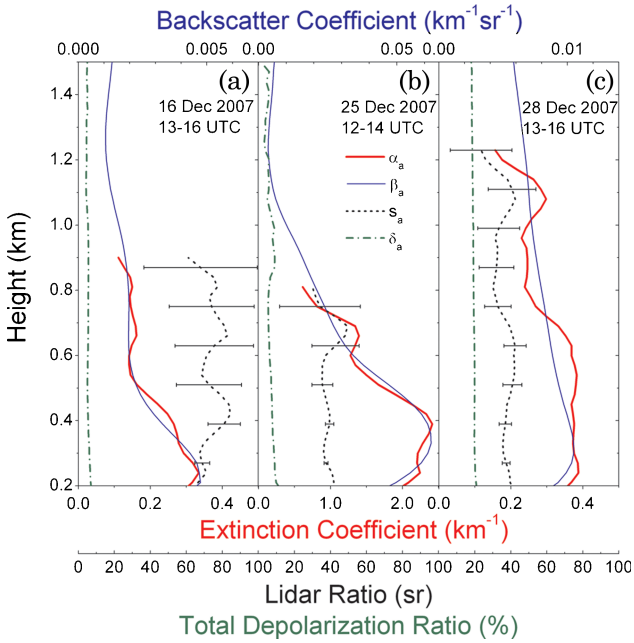

Fig. 2. (Color online) Vertical profiles of the aerosol extinction coefficient α_a (thick curves) and the backscatter coefficient β_a (thin curves) coefficients, the lidar ratio S_a (dotted curves), and the total depolarization ratio δ_a (dot–dashed curves) at 532 nm in the (a) moderate pollution, (b) heavy pollution, and (c) Asian dust episodes over Beijing. Error bars for lidar ratio indicate ±1 standard deviations due to the detection noise.

ending at 1200 UTC on 16 December was calculated using the NOAA HYSPLIT trajectory model [23] and is shown in Fig. 3(a). The backward trajectory shows the air mass was transported from the northwest where the air is relatively clean. It also shows the flow is not fast enough to get rid of accumulation of pollution in Beijing. As a result, dispersed air pollution [24] from anthropogenic sources (probably in Beijing) containing aerosols having a high lidar ratio, such as carbonaceous species [25], was observed during this event.

B. Heavy Pollution Episode

Figure 2(b) presents the optical properties of aerosols observed on 25 December in the heavy pollution episode. In this episode, the aerosol extinction coefficient below 0.8 km height exceeded 1 km^{-1}, and the maximum value reached 2.5 km^{-1} at 0.4 km height. The aerosol backscatter profile reached a height of about 2.5 km, but most of the pollution aerosol was below 0.8 km. The aerosol optical depth was 1.06 between 0.2 and 0.8 km. The derived lidar ratio was 38.5 ± 4.7 sr, and the total depolarization ratio was $7.22 \pm 1.37\%$.

Compared to the moderate pollution episode on 16 December, the aerosol extinction coefficient on 25 December was large and the lidar ratio was small. In addition, the ratio of the backscatter at 1064 nm to that at 532 nm (i.e., β_{1064}/β_{532}) was larger, indicating the presence of larger particles. The differences are probably due to the difference in the ambient meteorological conditions. A stable atmospheric condition with high relative humidity (84.5% on 25 December) continued during the heavy pollution episode, and the backward trajectory [Fig. 3(b)] indicates that the polluted aerosols were accumulated in the Beijing area. The lower lidar ratio was probably affected by hygroscopic growth of water-soluble aerosols such as sulfates and nitrates mixed in the air-pollution aerosols in Beijing [26].

C. Asian Dust Episode

Asian dust episodes are typically characterized by passage of cold fronts and relatively dry conditions and strong wind from the northwest. The data at the ZBAA Meteorological Station showed that relative humidity decreased sharply to 25% at 0600 UTC on 28 December. A strong northwesterly wind with a maximum wind speed exceeding 15 m/s prevailed from 28 to 30 December. Figure 2(c) presents the optical properties of Asian dust aerosols measured on 28 December. The aerosol extinction coefficient was 0.4 to 0.2 km^{-1} up to 1.2 km height. The derived backscatter profile indicates that the dust

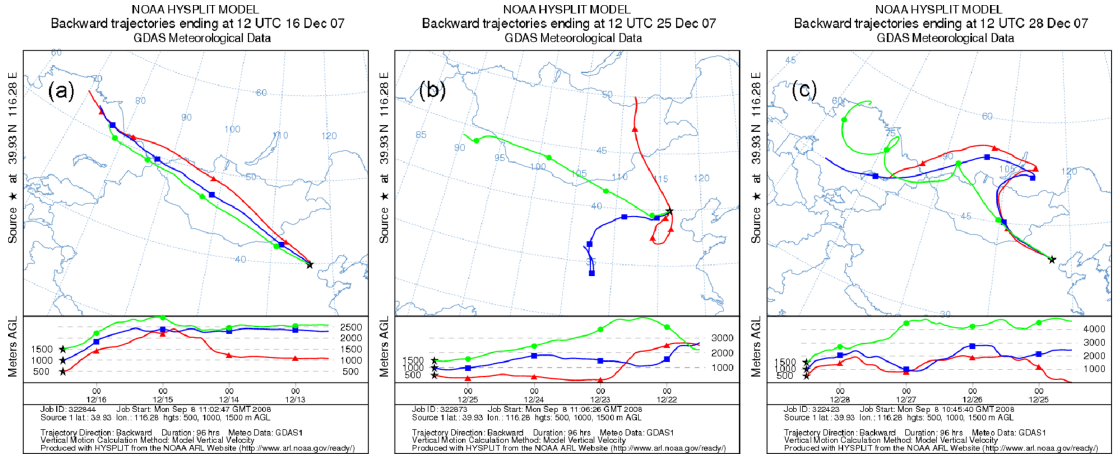

Fig. 3. (Color online) Backward trajectories calculated by the HYSPLIT model ending at Beijing on (a) 16 December in the moderate pollution episode, (b) 25 December in the heavy pollution episode, and (c) 28 December in the Asian dust episode.

aerosol reached a height of about 4 km. The lidar ratio was 36.2 ± 4.7 sr in the 0.2 to 1.2 km height range. The backscatter color ratio (β_{1064}/β_{532}) was relatively large, indicating the presence of large particles. The averaged total depolarization ratio was $19.54 \pm 0.53\%$. Thus, these results reasonably demonstrate the presence of nonspherical mineral dust particles.

In addition to the lidar observation, satellite data and backward trajectory analysis are useful for identifying the origin and transport of dust aerosols [2,27]. The NOAA-17 satellite image observed at 1110 LT on 28 December [28], not shown in this paper, indicates the dust storm occurred in Inner Mongolia, China. The HYSPLIT backward trajectory ending at 1200 UTC on 28 December [Fig. 3(c)] was the trajectory passed over the same area. The local meteorological station at Erlianhot in Inner Mongolia also reported the Asian dust event at 2100 LT on 27 December. The wind speed exceeded 7 m/s, and the local visibility was less than 0.5 km. All of these observations showed that this rare Asian dust event in winter was generated in Inner Mongolia on 27 December and transported to Beijing on the next day. The observed dust is not believed to be contaminated by pollution aerosol since the air flow was sufficiently fast to inhibit accumulation of pollution aerosols during transportation.

4. Summary and Discussion

Aerosol optical properties were measured with the NIES compact Raman lidar over Beijing, China, from 15 to 31 December 2007. We classified the situations in the observation period into three episodes (a moderate pollution episode from 15 to 17 December, a heavy pollution episode from 18 to 27 December, and an Asian dust episode from 28 to 30 December), according to the aerosol extinction coefficient and the meteorological data. Obvious differences in the aerosol optical properties were found in the three episodes (Fig. 4). The atmosphere in the moderate pollution episode was characterized by medium aerosol extinction coefficient (mean $= 0.39 \pm 0.15\,\mathrm{km}^{-1}$), high lidar ratio ($60.8 \pm 13.5$ sr), and low total depolarization ratio ($7.38 \pm 1.52\%$). In the heavy pollution, it was characterized by high aerosol extinction coefficient (mean $= 1.97 \pm 0.91\,\mathrm{km}^{-1}$), medium lidar ratio ($43.7 \pm 8.3$ sr), and low total depolarization ratio ($7.42 \pm 1.95\%$). In the Asian dust event, it was characterized by medium extinction coefficient (mean $= 0.33 \pm 0.11\,\mathrm{km}^{-1}$), medium lidar ratio ($38.3 \pm 9.8$ sr), and high total depolarization ratio ($20.3 \pm 3.0\%$).

In the Raman lidar observation in January 2005 in Beijing reported by Tesche *et al.* [11], the observed lidar ratio varied from 30 to 45 sr with a mean value of 38 ± 7 sr, and an unexpectedly low lidar ratio of 25 sr was found during their experiment. They concluded that the dry, clean conditions and the prevailing northwesterly air flow during their 11 day observation were the main reasons for the considerably smaller lidar ratio than those expected for anthropogenic aerosols. The mean lidar ratio for the Asian dust episode in the present experiment is comparable to the mean lidar ratio reported by Tesche *et al.* We have not observed, however, a clean background atmosphere having a very low lidar ratio. The lidar ratio for the relatively clear case we observed on 31 December was approximately 60 sr in the boundary layer.

The lidar ratios in the moderate and heavy pollution episodes are comparable to those reported for air-pollution aerosols in Southeast Asia [9,29]. The lidar ratio of 43.7 sr observed in the heavy pollution episode was smaller than that of 60.8 sr in the

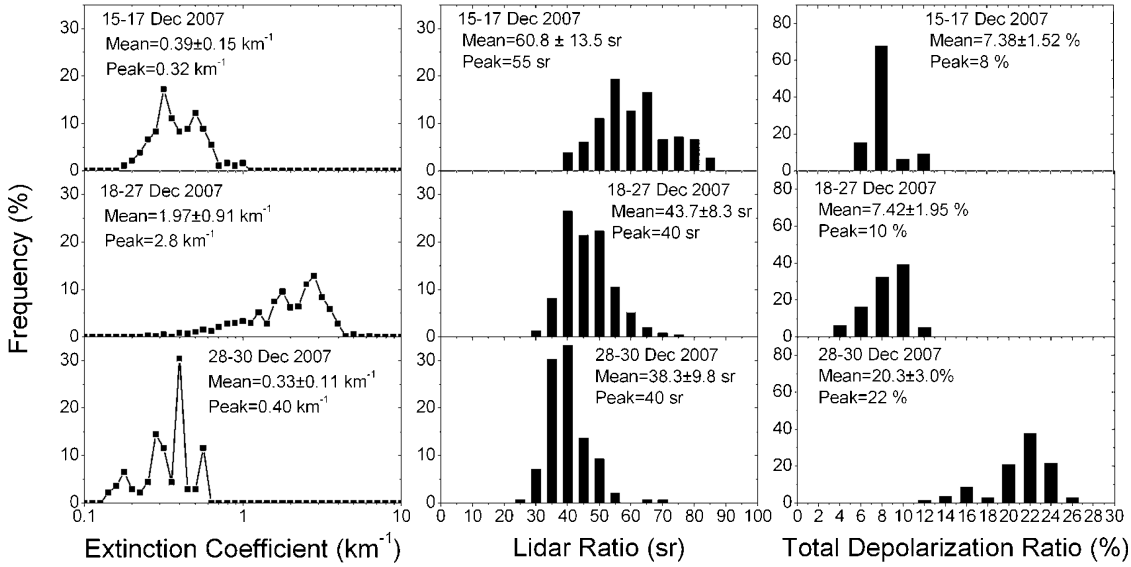

Fig. 4. Frequency distributions of the aerosol extinction coefficient, the lidar ratio, and the total depolarization ratio in the 0.2–1 km height range during the moderate pollution episode (15–17 December), heavy pollution episode (18–27 December), and Asian dust episode (28–30 December) in Beijing. The derived optical parameters between 0.2 and 1 km height with errors less than 50% are shown in the figure.

moderate pollution episode. This is probably affected by hygroscopic growth of aerosols due to the high relative humidity in the heavy pollution episode as mentioned in the previous section. The larger value of backscatter color ratio (β_{1064}/β_{532}) observed with the NIES Raman lidar is qualitatively consistent with this explanation.

The lidar ratio in the heavy pollution episode is close to that of the haze-layer aerosol in the south of China in October 2004 (46.7 sr) reported by Ansmann *et al.* [16]. They also reported low values of the Angstrom exponent at high relative humidity, implying the presence of large particles and the effect of the hygroscopic growth on the pollution aerosol.

The dust lidar ratio of 38.3 sr in this study is consistent with the reported values for Asian dust (36 to 70 sr) [30–34] but is a little lower. This may be closely related to various processes occurring in long-range transportation such as gravity settling and internal and/or external mixing [35,36]. The observation site in this study is relatively close to the dust source area, while most of the previous Asian dust lidar ratio observations have been conducted in areas far from the dust source (e.g., Japan, Korea, and Taiwan). Papayannis *et al.* [37] estimated a column lidar ratio of 84 sr for a heavy Asian dust event over Beijing in April 2006 by the combined use of Sun photometer and elastic lidar data. The reported dust lidar ratio is considerably larger than those in this study and the other studies, probably due to contamination by other aerosol types [38] and the different retrievals of dust lidar ratio.

Aerosols in Beijing are a complex mixture of various anthropogenic aerosols and transported mineral dust particles. The observed lidar ratio is determined by the mixing state of aerosols, which is dependent on the history of the air mass. To study further the characteristics of aerosols in Beijing, we continue the Raman lidar observation and also plan collaboration with *in situ* and sampling measurements of microphysical properties of aerosols such as size distributions and aerosol types.

This work was supported by the Global Environment Research Fund of the Ministry of the Environment, Japan (C-061). The radiosonde data used in this paper were produced from NOAA's database at http://raob.fsl.noaa.gov/, and the surface meteorological data, from the University of Wyoming website at http://weather.uwyo.edu/wyoming/.

References

1. J. Liu and J. Diamond, "China's environment in a globalizing world," Nature **435**, 1179–1186 (2005).
2. T. Murayama, N. Sugimoto, I. Uno, K. Kinoshita, K. Aoki, N. Hagiwara, Z. Liu, I. Matsui, T. Sakai, T. Shibata, K. Arao, B. J. Sohn, J. G. Won, S. C. Yoon, T. Li, J. Zhou, H. Hu, M. Abo, K. Iokibe, R. Koga, and Y. Iwasaka, "Ground-based network observation of Asian dust events of April 1998 in east Asia," J. Geophys. Res. **106**, 18345–18359 (2001).
3. A. Ansmann, M. Riebesell, U. Wandinger, C. Weitkamp, E. Voss, W. Lahmann, and W. Michaelis, "Combined Raman elastic-backscatter LIDAR for vertical profiling of moisture, aerosol extinction, backscatter and LIDAR ratio," Appl. Phys. B **55**, 18–28 (1992).
4. V. Matthias, D. Balis, J. Bösenberg, R. Eixmann, M. Iarlori, L. Komguem, I. Mattis, A. Papayannis, G. Pappalardo, M. R. Perrone, and X. Wang, "Vertical aerosol distribution over Europe: statistical analysis of Raman lidar data from 10 European Aerosol Research Lidar Network (EARLINET) stations," J. Geophys. Res. **109**, D18201 (2004).
5. U. Wandinger, I. Mattis, M. Tesche, A. Ansmann, J. Bösenberg, A. Chaikovski, V. Freudenthaler, L. Komguem, H. Linné, V. Matthias, J. Pelon, L. Sauvage, P. Sobolewski, G. Vaughan, and M. Wiegner, "Air mass modification over Europe: EARLINET aerosol observations from Wales to Belarus," J. Geophys. Res. **109**, D24205 (2004).
6. L. Mona, A. Amodeo, M. Pandolfi, and G. Pappalardo, "Saharan dust intrusions in the Mediterranean area: Three years of Raman lidar measurements," J. Geophys. Res. **111**, D16203 (2006).
7. K. Franke, A. Ansmann, D. Müller, D. Althausen, C. Venkataraman, M. S. Reddy, F. Wagner, and R. Scheele, "Optical properties of the Indo-Asian haze layer over the tropical Indian Ocean," J. Geophys. Res. **108**, 4059 (2003).
8. D. Müller, K. Franke, F. Wagner, D. Althausen, A. Ansmann, and J. Heintzenberg, "Vertical profiling of optical and physical particle properties over the tropical Indian Ocean with six-wavelength lidar 1. Seasonal cycle," J. Geophys. Res. **106**, 28567–28575 (2001).
9. D. Müller, K. Franke, F. Wagner, D. Althausen, A. Ansmann, J. Heintzenberg, and G. Verver, "Vertical profiling of optical and physical particle properties over the tropical Indian Ocean with six-wavelength lidar 2. Case studies," J. Geophys. Res. **106**, 28577–28595 (2001).
10. D. D. Turner, R. A. Ferrare, L. A. H. Brasseur, and W. F. Feltz, "Automated retrievals of water vapor and aerosol profiles from an operational Raman lidar," J. Atmos. Ocean. Technol. **19**, 37–50 (2002).
11. M. Tesche, A. Ansmann, D. Müller, D. Althausen, R. Engelmann, M. Hu, and Y. Zhang, "Particle backscatter, extinction, and lidar ratio profiling with Raman lidar in south and north China," Appl. Opt. **46**, 6302–6308 (2007).
12. N. Sugimoto, I. Uno, M. Nishikawa, A. Shimizu, I. Matsui, X. Dong, Y. Chen, and H. Quan, "Record heavy Asian dust in Beijing in 2002: observations and model analysis of recent events," Geophys. Res. Lett. **30**, 1640 (2003).
13. A. Shimizu, N. Sugimoto, I. Matsui, K. Arao, I. Uno, T. Murayama, N. Kagawa, K. Aoki, A. Uchiyama, and A. Yamazaki, "Continuous observations of Asian dust and other aerosols by polarization lidars in China and Japan during ACE-Asia," J. Geophys. Res. **109**, D19S17 (2004).
14. K. Sassen, "The polarization lidar technique for cloud research: a review and current assessment," Bull. Am. Meteorol. Soc. **72**, 1848–1866 (1991).
15. T. Murayama, H. Okamoto, N. Kaneyasu, H. Kamataki, and K. Miura, "Application of lidar depolarization measurement in the atmospheric boundary layer: effects of dust and sea-salt particles," J. Geophys. Res. **104**, 31781–31792 (1999).
16. A. Ansmann, R. Engelmann, D. Althausen, U. Wandinger, M. Hu, Y. Zhang, and Q. He, "High aerosol load over the Pearl River Delta, China, observed with Raman lidar and Sun photometer," Geophys. Res. Lett. **32**, L13815 (2005).
17. D. Müller, A. Ansmann, F. Wagner, K. Franke, and D. Althausen, "European pollution outbreaks during ACE 2: microphysical particle properties and single-scattering albedo inferred from multiwavelength lidar observations," J. Geophys. Res. **107**, 4248 (2002).

18. D. Müller, K. Franke, A. Ansmann, D. Althausen, and F. Wagner, "Indo-Asian pollution during INDOEX: Microphysical particle properties and single-scattering albedo inferred from multiwavelength lidar observations," J. Geophys. Res. **108**, 46002003.
19. D. Müller, I. Mattis, U. Wandinger, A. Ansmann, D. Althausen, and A. Stohl, "Raman lidar observations of aged Siberian and Canadian forest fire smoke in the free troposphere over Germany in 2003: microphysical particle characterization," J. Geophys. Res. **110**, D17201(2005).
20. U. Wandinger and A. Ansmann, "Experimental determination of the lidar overlap profile with Raman lidar," Appl. Opt. **41**, 511–514 (2002).
21. A. Ansmann, D. Althausen, U. Wandinger, K. Franke, D. Müller, F. Wagner, and J. Heintzenberg, "Vertical profiling of the India aerosol plume with six-wavelength lidar during INDOEX: a first case study," Geophys. Res. Lett. **27**, 963–966 (2000).
22. X. Xu, J. Gao, D. W. Dockery, and Y. Chen, "Air pollution and daily mortality in residential areas of Beijing, China," Arch. Environ. Health **49**, 216–222 (1994).
23. R. R. Draxler and G. D. Rolph, "Hybrid Single-Particle Lagrangian Integrated Trajectory (HYSPLIT)," obtained from the National Oceanic and Atmospheric Administration's Air Resources Laboratory via http://www.arl.noaa.gov/ready/hysplit4.html (2007).
24. C. J. Walcek, "Effects of wind shear on pollution dispersion," Atmos. Environ. **36**, 511–517 (2002).
25. M. Dan, G. Zhuang, X. Li, H. Tao, and Y. Zhuang, "The characteristics of carbonaceous species and their sources in PM2.5 in Beijing," Atmos. Environ. **38**, 3443–3452 (2004).
26. I. N. Tang, "Chemical and size effects of hygroscopic aerosols on light scattering coefficients," J. Geophys. Res. **101**, 19245–19250 (1996).
27. N. Murayama, "Dust cloud "Kosa" from the East Asian dust storms in 1982–1988 as observed by the GMS satellite," Meteorol. Satell. Cent. Tech. Note **17**, 1–8 (1998).
28. The NSMC, NOAA-17 satellite image was produced by the National Satellite Meteorological Center (NSMC) of China Meteorological Administration and was found at the website of the China dust storm monitoring network, http://www.dustst orm.com.cn, 2007.
29. C. Cattrall, J. Reagan, K. Thome, and O. Dubovik, "Variability of aerosol and spectral lidar and backscatter and extinction ratios of key aerosol types derived from selected Aerosol Robotic Network locations," J. Geophys. Res. **110**, D10S11 (2005).
30. Z. Liu, N. Sugimoto, and T. Murayama, "Extinction-to-backscatter ratio of Asian dust observed with high-spectral-resolution lidar and Raman lidar," Appl. Opt. **41**, 2760–2767 (2002).
31. T. Murayama, "Optical properties of Asian dust aerosol lofted over Tokyo observed by Raman lidar," in *Lidar Remote Sensing in Atmospheric and Earth Science*, L. R. Bissonnette, G. Roy, and G. Vallée, eds. (Defence R&D Canada, Québec, Canada, 2002), pp. 331–334.
32. Y. M. Noh, Y. J. Kim, B. C. Choi, T. and Murayama, "Aerosol lidar ratio characteristics measured by a multi-wavelength Raman lidar system at Anmyeon island, Korea," Atmos. Res. doi:10.1016/j.atmosres.2007.03.006 (2007).
33. B. Tatarov, N. Sugimoto, I. Matsui, and A. Shimizu, "Two-year-observations of optical properties of the tropospheric aerosol and clouds by a high-spectral-resolution lidar over Tsukuba, Japan," in *Reviewed and Revised Papers Presented at the 23rd International Laser Radar Conference* (publisher, 2006), pp. 451–454.
34. T. Murayama and M. Sekiguchi, "Intercomparison of aerosol optical properties observed by lidar, Sun/sky photometers and surface *in situ* measurements during Asian dust event in Tokyo, Japan," in *Reviewed and Revised Papers Presented at the 24th International Laser Radar Conference* (publisher, 2008), pp. 943–946.
35. N. Sugimoto, I. Matsui, A. Shimizu, I. Uno, K. Asai, T. Endoh, and T. Nakajima, "Observation of dust and anthropogenic aerosol plumes in the Northwest Pacific with a two-wavelength polarization lidar on board the research vessel Mirai," Geophys. Res. Lett. **29**, 1901 (2002).
36. Y. Iwasaka, G.-Y. Shi, M. Yamada, A. Matsuki, D. Trochkine, Y. S. Kim, D. Zhang, T. Nagatani, T. Shibata, M. Nagatani, H. Nakata, Z. Shen, G. Li, and B. Chen, "Importance of dust particles in the free troposphere over the Taklamakan Desert: electron microscopic experiments of particles collected with a balloonborne particle impactor at Dunhuang, China," J. Geophys. Res. **108**, 8644 (2003).
37. A. Papayannis, H. Q. Zhang, V. Amiridis, H. B. Ju, G. Chourdakis, G. Georgoussis, C. Pérez, H. B. Chen, P. Goloub, R. E. Mamouri, S. Kazadzis, D. Paronis, G. Tsaknakis, and J. M. Baldasano, "Extraordinary dust event over Beijing, China, during April 2006: lidar, sun photometric, satellite observations and model validation," Geophys. Res. Lett. **34**, L07806 (2007).
38. A. Ansmann, "Ground-truth aerosols lidar observations: can the Klett solutions obtained from ground and space be equal for the same aerosol case?," Appl. Opt. **45**, 3367–3371 (2006).